

State-selective single- and double-electron capture in collisions of low-energy S^{5+} ions with helium

Yixin Fan(樊依鑫), Dadi Xing(邢大地), Shucheng Cui(崔述成), Xiaoxia Wang(王小霞), Junxia Ran(冉俊霞), Kaizhao Lin(林楷钊), Xubin Zhu(朱旭斌), Dongmei Zhao(赵冬梅), Dalong Guo(郭大龙), Yong Gao(高永), Shaofeng Zhang(张少锋), Xiaolong Zhu(朱小龙), and Xinwen Ma(马新文)

Citation: Chin. Phys. B, 2025, 34 (**7**): 073402. DOI: 10.1088/1674-1056/adcb9a
http://cpb.iphy.ac.cn; http://iopscience.iop.org/cpb

What follows is a list of articles you may be interested in

Theoretical study of differential cross sections for the ionization of helium by fast proton impact

M Mondal, B Mandal, T Mistry, D Jana, and M Purkait
Chin. Phys. B, 2024, 33 (**11**): 113401. DOI: 10.1088/1674-1056/ad74e6

Electron capture and excitation in intermediate-energy He^{2+}-H(1s,2s) collisions

Yadong Liu(刘亚东), Congcong Jia(贾聪聪), Mingxuan Ma(马茗萱), Xiang Gao(高翔), Ling Liu(刘玲), Yong Wu(吴勇), Xiangjun Chen(陈向军), and Jianguo Wang(王建国)
Chin. Phys. B, 2024, 33 (**8**): 083401. DOI: 10.1088/1674-1056/ad5322

The *n*-resolved single-electron capture in slow O^{6+}-Ne collisions

Shucheng Cui(崔述成), Dadi Xing(邢大地), Xiaolong Zhu(朱小龙), Maogen Su(苏茂根), Yong Gao(高永), Dalong Guo(郭大龙), Dongmei Zhao(赵冬梅), Shaofeng Zhang(张少锋), Yanbiao Fu(符彦飙), and Xinwen Ma(马新文)
Chin. Phys. B, 2024, 33 (**7**): 073401. DOI: 10.1088/1674-1056/ad39d2

State-selective charge exchange cross sections in collisions of highly-charged sulfur ions with helium and molecular hydrogen

Xiaolong Zhu(朱小龙), Shucheng Cui(崔述成), Dadi Xing(邢大地), Jiawei Xu(徐佳伟), B. Najjari, Dongmei Zhao(赵冬梅), Dalong Guo(郭大龙), Yong Gao(高永), Ruitian Zhang(张瑞田), Maogen Su(苏茂根), Shaofeng Zhang(张少锋), and Xinwen Ma(马新文)
Chin. Phys. B, 2024, 33 (**2**): 023401. DOI: 10.1088/1674-1056/ad0b01

Charge transfer in low-energy collisions ofBe^{3+} and B^{4+} ions with He

Kun Wang(王堃), Yi-Zhi Qu(屈一至), Chun-Hua Liu(刘春华), Ling Liu(刘玲), Yong Wu(吴勇), H P Liebermann, Robert J. Buenker
Chin. Phys. B, 2020, 29 (**9**): 093401. DOI: 10.1088/1674-1056/aba276

DATA PAPER

State-selective single- and double-electron capture in collisions of low-energy S^{5+} ions with helium

Yixin Fan(樊依鑫)[1,2], Dadi Xing(邢大地)[2], Shucheng Cui(崔述成)[3], Xiaoxia Wang(王小霞)[4,†], Junxia Ran(冉俊霞)[1,‡], Kaizhao Lin(林楷钊)[2], Xubin Zhu(朱旭斌)[2,5], Dongmei Zhao(赵冬梅)[2], Dalong Guo(郭大龙)[2,5], Yong Gao(高永)[2,5], Shaofeng Zhang(张少锋)[2,5,6], Xiaolong Zhu(朱小龙)[2,5,6,§], and Xinwen Ma(马新文)[2,5,6]

[1] *College of Physics Science and Technology, Hebei University, Baoding* 071002, *China*
[2] *Institute of Modern Physics, Chinese Academy of Sciences, Lanzhou* 730000, *China*
[3] *College of Physics and Electronic Engineering, Northwest Normal University, Lanzhou* 730070, *China*
[4] *College of Physics, Chendu University of Technology, Chengdu* 610059, *China*
[5] *University of Chinese Academy of Sciences, Beijing* 100049, *China*
[6] *State Key Laboratory of Heavy Ion Science and Technology, Institute of Modern Physics, Chinese Academy of Sciences, Lanzhou* 730000, *China*

(Received 22 January 2025; revised manuscript received 26 March 2025; accepted manuscript online 11 April 2025)

State-selective single- and double-electron capture processes in collisions of S^{5+} ions with helium at energies ranging from 50.8 keV to 100 keV were investigated using cold target recoil ion momentum spectroscopy (COLTRIMS). Q-value spectra and projectile scattering angle distributions were obtained. For single-electron capture, single electron capture into $n = 3$ states of the projectile ion is dominant. As the projectile energy increases, the contribution of single electron capture into $n = 4$ states is observed. Experimental relative cross-sections for single-electron capture into different projectile final states were compared with theoretical predictions based on the molecular orbital close-coupling (MOCC) method. In double-electron capture, two-electron populating into the $3s^23p$ and $3s3p^2$ states of projectile dominates. The reaction window calculated from the classical molecular Coulombic barrier model can qualitatively explain the experimental results. The scattering angle distribution of the multi-peak structure of the double-electron capture process is observed. The database is openly available in Science Data Bank at https://doi.org/10.57760/sciencedb.j00113.00233.

Keywords: state-selective electron-capture, sulfur ion, low-energy collisions, cold target recoil ion momentum spectroscopy (COLTRIMS)

PACS: 34.70.+e, 95.30.Dr

DOI: 10.1088/1674-1056/adcb9a **CSTR:** 32038.14.CPB.adcb9a

1. Introduction

Electron capture in ion–atom collisions represents a fundamental process in atomic physics. In fundamental research, electron capture processes contribute to our understanding of atomic structure and the few-body dynamical mechanisms, such as electron–electron correlations and strong Coulomb interactions.[1] Furthermore, in applied research, electron capture processes play a crucial role in astrophysics, plasma physics, biological irradiation effects, etc.[2–5] The pure electron capture process can be simply represented by the following equation:

$$A^{q+} + B \longrightarrow A^{(q-n)+} + B^{n+}, \tag{1}$$

where A is the projectile ion, q is its charge state, B is the target atom, and n is the number of electrons captured by the projectile ion during the collision. The process with $n = 1$ is called single-electron capture (SEC), and that with $n = 2$ is called double-electron capture (DEC). The review paper discusses the progress and challenges of atomic structure and collision dynamics with highly charged ions.[6] Experimental breakthroughs have been achieved in characterizing state-selective SEC and DEC processes for highly charged ions (including Ar^{8+}, Ne^{8+}, Ne^{7+}, O^{6+}, O^{4+}, C^{3+}, and N^{5+}) through advanced detection techniques with cold target recoil ion momentum spectroscopy (COLTRIMS) and high-resolution reaction microscopes.[7–16] Theoretical frameworks have correspondingly evolved, with two distinct computational approaches demonstrating particular efficacy: The two-center atomic orbital close-coupling (TC-AOCC) method has successfully modeled SEC mechanisms in Ne^{q+}–H collisions (q = 6–10),[17] while both TC-AOCC and single-center atomic orbital close-coupling (SC-AOCC) methodologies have provided insights into SEC and DEC dynamics for C^{4+}–He[18] and Ar^{8+}–He.[19] Notably, synergistic experimental–theoretical investigations have further eluci-

†Corresponding author. E-mail: wangxx@cdut.edu.cn
‡Corresponding author. E-mail: rjxhbu@hbu.cn
§Corresponding author. E-mail: zhuxiaolong@impcas.ac.cn

© 2025 Chinese Physical Society and IOP Publishing Ltd. All rights, including for text and data mining, AI training, and similar technologies, are reserved.

dated collision processes in Ar^{8+}–He,[7] Ar^{8+}–H_2,[13] O^{6+}–He[14] and C^{3+}–He[15] collision systems, establishing robust cross-validation between empirical observations and computational predictions.

Sulfur ions, as significant heavy ions, are ubiquitously observed in astrophysical environments, including the solar wind, interstellar medium, and galaxy clusters.[20–23] Many astronomical studies have shown that electron capture processes between heavy ions, like sulfur ions, and neutral atmosphere are the main source of x-rays.[24,25]

Due to the importance of sulfur ions, Wilson *et al.* investigated the state selective electron capture of slow S^{2+} ions from a recoil ion source using translational energy spectroscopy.[26] To understand the dynamic mechanisms further, Zhao *et al.* conducted a comparative study of electron capture in collisions of S^{2+} ions with He atoms at collision energies between 2.5 eV/u and 10 keV/u using fully quantum molecular orbitals close coupling method (QMOCC) and semiclassical molecular orbitals close coupling method (SCMOCC).[27] Subsequently, Wilson *et al.* measured the state selective electron capture cross sections of S^{3+} ions from H, H_2 and He at collision energies between 2.4 keV and 9.0 keV. For the H and He targets, a multichannel Landau–Zener (MCLZ) model was used to predict the cross sections.[28] Besides, Bacchus *et al.* studied the SEC process of the S^{3+}–He collision system at the laboratory energy range of 2–50 keV using a semiclassical approach. The results are in good agreement with experimental data.[29] Labuda *et al.* reported a theoretical study of state selective SEC in collisions of S^{3+} ions with H and He atoms at low collision energies, also using a semiclassical approach.[30,31] Wang *et al.* carried out a theoretical study of the electron capture process in collisions of ground-state S^{4+} ($3s^2\ ^1S$) ions with He energies ranging from 0.1 meV/u to 10 MeV/u. By using quantum mechanical molecular-orbital close-coupling (QMOCC), atomic-orbital close-coupling (AOCC), classical trajectory Monte Carlo (CTMC), and continuous distorted wave methods, they obtained the total cross-section and the state selective electron capture cross sections for the SEC process as well as the rate coefficients.[32] Zhu *et al.* pioneered the investigation of state-selective single-electron capture processes in S^{q+}–He and S^{q+}–H_2 collisions (q = 11–15) at $20 \cdot q$ keV energies using COLTRIMS.[1,33] Their work provided the first experimental determination of the principal quantum number n distribution and yielded relative state-selective cross sections for these systems.[34]

However, there have been no reports of experimental studies of state-selective electron capture in S^{5+} ions. In the present work, we investigated the state-selective single- and double-electron capture processes in S^{5+}–He collisions at impact energies from 50.8 keV to 100 keV using the COLTRIMS and obtained Q-value spectra and scattering angle distributions. The measured results were qualitatively interpreted using the molecular Coulomb barrier model (MCBM)[35] and potential energy curves. Unless otherwise indicated, atomic units are used.

2. Experimental setup

The experiments were conducted using the COLTRIMS at the EBIS-A facility at the Institute of Modern Physics, Chinese Academy of Sciences, Lanzhou, China, the details can be found elsewhere.[36] A brief introduction is provided here. The facility includes a EBIS-A ion source, a high voltage platform with deceleration lens, a Wien filter and a beam guiding and diagnostic system. Projectile ions are produced and extracted from the EBIS-A ion source, and can be analyzed by the Wien filter. Then, they are accelerated or decelerated to the required energy on the high voltage platform. The accelerated or decelerated ions are guided to the experimental terminal for different experiments. Our COLTRIMS experimental apparatus and methods are described in previous literatures.[34,36–40] S^{5+} ions generated and extracted from EBIS-A are accelerated and collided with a supersonic helium beam at the geometric center of the time-of-flight (TOF). The scattered ion charge states were analyzed using an electrostatic analyzer with a position-sensitive detector (PSD) equipped with delay-line anode, and the recoil target ions were guided to another position-sensitive detector by an electric field perpendicular to the projectile beam and target beam. S^{5+} ions not involved in the collision are collected by the Faraday cup. In addition, the experiment employs the recoil and scattering ion coincident technique, which allows individual reaction events in the collision process to be obtained one by one, thus effectively separating the different reaction processes.

3. Results and discussion

The longitudinal (along the ion beam direction) and transverse (perpendicular to the ion beam direction) momentum of the recoil ions can be reconstructed. For the pure electron capture process, according to the energy and momentum conservations, the Q value and θ can be determined by

$$P_{\text{long}} = -\frac{Q}{v_{\text{p}}} - \frac{1}{2} \cdot n \cdot v_{\text{p}}, \tag{2}$$

$$P_{\text{trans}} = P_0 \cdot \theta, \tag{3}$$

where Q is the difference in binding energy of the active electrons before and after the collision, n is the number of captured electrons, v_{p} is the velocity of the projectile, P_0 is the initial momentum of the projectile ion, and θ is the scattering angle of the projectile ion. The Q value reveals the information about the populated state of electron, and the angular distribution reveals the information about the dynamics of the electron capture.

3.1. SEC in S^{5+}–He collisions

Figure 1 shows the measured Q-value spectra of SEC in S^{5+}–He collision for impact energies of 50.8 keV and 100 keV. The populated states of the captured electron are shown in Fig. 1, which correspond to $nln'l'$ in

$$S^{5+}(3s) + He \longrightarrow S^{4+}(nln'l') + He^{+}(1s). \tag{4}$$

The formation of $S^{4+}(3p^2)$ involves the transfer projectile excitation (TPE) process where the S^{5+} projectile ion captures one electron from the He target to its 3p orbitals, accompanied by the projectile excitation of 3s into 3p orbitals. Spectral term resolution of ^{2S+1}L is implemented, e.g., 3s3p ^{3}P^o, 3s3p ^{1}P^o, and so on. Relative state-selective cross sections were derived by applying Gaussian fits to the Q-value spectra of the SEC process, as shown in Table 1. It can be seen that projectile ions capture electrons into 3l orbitals and TPE dominates the SEC process. As the energy increases, there is a small increase in the contribution of captured electrons to $n = 4$ states and the reaction window expands, as predicted by the MCBM model.

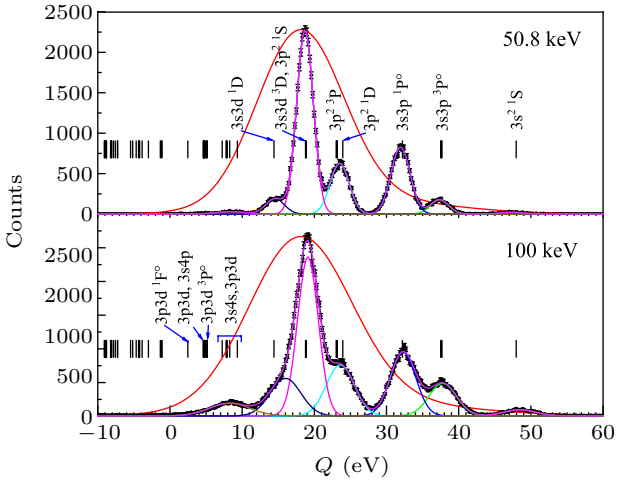


Fig. 1. The Q-value spectra of SEC in S^{5+}–He collision. The black vertical line is the scattering ion extranuclear electron fabrication for the SEC process, red curve is the reaction window calculated by the MCBM model,[35] and color curves are the results obtained from Gaussian fit.

Table 1. State-selective SEC relative cross-sections measured in S^{5+}–He collision. The error bars are determined from the Gaussian fitting error of the peaks and the collection range of the solid angle by the recoil detector.

	3s^2 ^{1}S	3s3p ^{3}P^o	3s3p ^{1}P^o	3p^2 ^{1}D, 3p^2 ^{3}P	3s3d ^{3}D, 3p^2 ^{1}S	3s3d ^{1}D	3s4s, 3p3d, 3s4p
50.8 keV	0.7 ± 0.1	4.4 ± 0.1	21.5 ± 0.2	16.2 ± 0.1	51.3 ± 0.3	4.8 ± 0.1	1.2 ± 0.1
100 keV	2.1 ± 0.1	9.9 ± 0.4	17.7 ± 0.6	15.7 ± 0.6	36.3 ± 1.5	12.6 ± 1.3	5.6 ± 0.3

Figure 2(a) shows the simplified potential energy curves[41] of the main reaction channels for the SEC process in S^{5+}–He collisions. For the incoming channel, the polarization potential between the projectile ion and the target is ignored. For the outgoing channels, similar to the treatment of Fischer *et al.*,[41] the kinetic energy of the captured electron and the Coulomb potential between the scattered ion and the recoil ion are considered as follows:

$$E = \frac{q_1 q_2}{r} - Q + \frac{n}{2} \cdot v_p{}^2, \tag{5}$$

where q_1 and q_2 are the charge states of the scattering and recoil ions, r is the nuclear distance between the projectile and the target nucleus, v_p is the projectile velocity and n is the number of captured electrons. For the SEC process, $n = 1$ and $n = 2$ for the DEC process. As can be seen from Fig. 2(a), the crossings of the incoming and outgoing channels may indicate the capture and TPE processes observed in our experiment. In addition, the electron structures of S^{5+}–He were obtained from the multi-reference single- and double-excitation configuration interaction (MRDCI) program.[42,43] The charge transfer processes were studied using the quantum-mechanical molecular-orbital close-coupling (QMOCC) method.[44–47] The potential energy curves are shown in Fig. 2(b). To describe the incoming state better, 47 potential energy curves of S^{5+}–He were calculated from 1.0 a.u. to 50.0 a.u. As for the choice of basis set, the effective core potential (ECP) and [4s, 4p] Gaussian-type basis set of CRENBL augmented by (2d, 2f) functions were used to describe the S atom. Aug-cc-pVDZ (augmented correlation consistent polarization valence quadruple ζ) basis set diffused by a set of (1s, 1p) functions was employed for the He atom. In the dynamical process, 17 reaction channels for S^{5+}–He collision were taken into consideration. Namely, the QMOCC calculation of S^{5+}–He is converged in this work.

The avoided crossing point of the incoming and outgoing channels for the 3p^2 ^{1}S and 3s3d ^{3}D states can be seen in the figure, which confirms the experimental result that the SEC process is dominated by the TPE and the capture of electrons into the 3s3d ^{3}D state. The relative cross sections of the main reaction channels in the SEC process from the experiment were compared with the results of the present theoretical calculations, as shown in Fig. 3. The colored solid lines in Fig. 3 represent the results of the theoretical calculations, and the colored points represent the experimental measurements. In Fig. 3, the main reaction channels represented by the black solid line, the red solid line, and the purple solid line are in good agreement with our experimental results. The purple diamond-shaped points represent the most important reaction channels 3s3d ^{3}D, 3p^2 ^{1}S in the experimental SEC process, and the theoretical calculated relative cross-sections are also in good agreement with the experimental results.

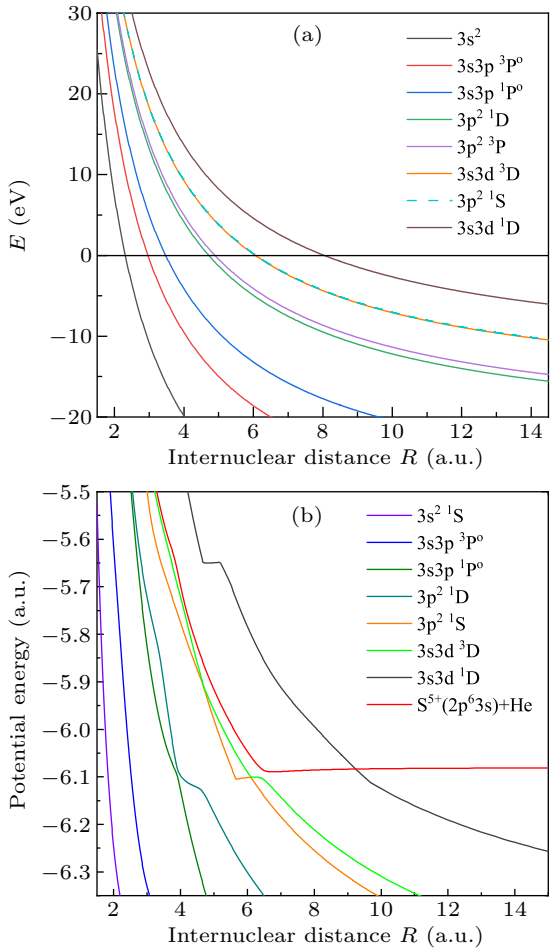


Fig. 2. (a) Potential energy curves for SEC process of S^{5+}–He collision at the energy of 50.8 keV by Eq. (5). (b) Potential energy curves of the S^{5+}–He collision system calculated by the QMOCC method, with the red solid line representing the incoming channel of the S^{5+} projectile ions and the other colored solid lines representing the outgoing channel of the projectile after capturing one electron.

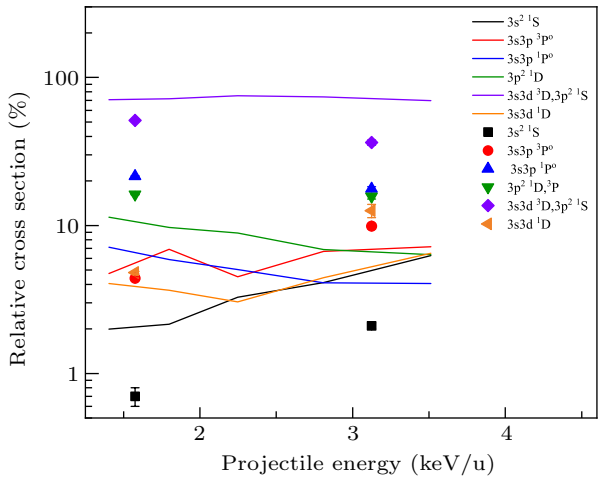


Fig. 3. Relative cross-sections of SEC channels in the S^{5+}–He collision, colored solid lines are the results obtained by the QMOCC method, and colored points represent experimental results.

The green solid line only considers the reaction channel $3p^2\ ^1D$, while our experimental measurements include both $3p^2\ ^1D$ and $3p^2\ ^3P$, which cannot be completely separated by experimental resolution due to the energy levels differing by less than 1 eV. The green curve, which accounts solely for the $3p^2\ ^1D$ state contribution, exhibits significant discrepancies compared to the present experimental data. Overall, the theoretical calculations are basically consistent with the experimental results in the dominant reaction channels, with deviations in the $3s3p\ ^1P^o$ channel and higher excited states, which may require more accurate theory for further explanation. Figure 4 shows the measured angular distributions of the SEC process for different final states, clearly demonstrating the bimodal structure.

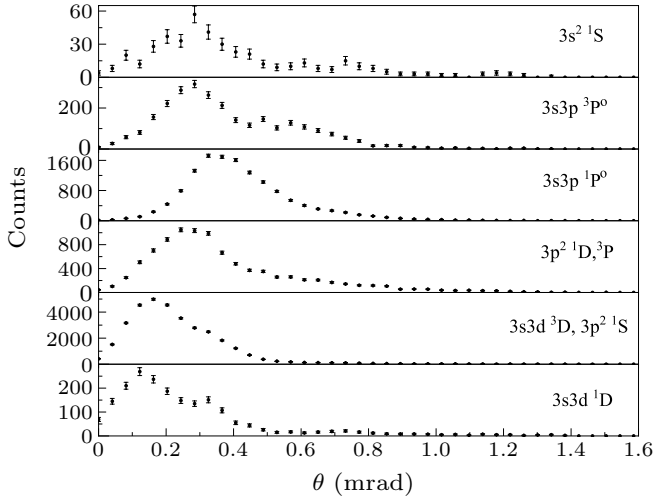


Fig. 4. Measured angular distributions in the final states of the SEC process at 50.8 keV collision energy.

3.2. DEC in S^{5+}–He collisions

Figure 5 shows the measured Q-value spectra of DEC in S^{5+}–He collisions at 50.8 keV and 100 keV impact energies. The captured channels shown in Fig. 5 are as follows:

$$S^{5+}(3s) + He \longrightarrow S^{3+}(nln'l'n''l'') + He^{2+}. \tag{6}$$

Similar to SEC, the final states are corresponding to $nln'l'n''l''$ in Eq. (6). It can be seen that the DEC process is dominated by the capture of double-electron into the ground state $3s^23p$, but the capture of electrons to the $3s3p^2$ state is also significant. Figure 5 shows that channels in higher excited states such as $3s^23d$, $3s^24s$ are opened as the collision energy rises. It is noteworthy that the $3s3p^2\ ^2P$ state at an impact energy of 50.8 keV is in the position of the trough, meaning that no capture of electrons to the $3s3p^2\ ^2P$ state occurs, but at 100 keV we can see some contribution from this channel. Nevertheless, the capture of electrons into the ground state $3s^23p$ remains the dominant reaction channel. The predictions of MCBM agree qualitatively with the present experimental results. Figure 6 shows the measured angular distributions of the DEC process in the final states and demonstrates the obviously multi-modal structure.

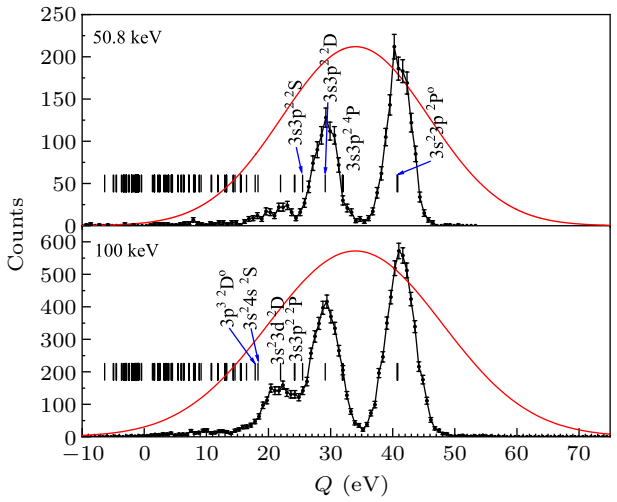


Fig. 5. The Q-value spectra of DEC in S^{5+}–He collision. The black vertical line is the scattering ion extranuclear electron fabrication for the DEC process, and the red curve is the reaction window calculated by the MCBM model.[35]

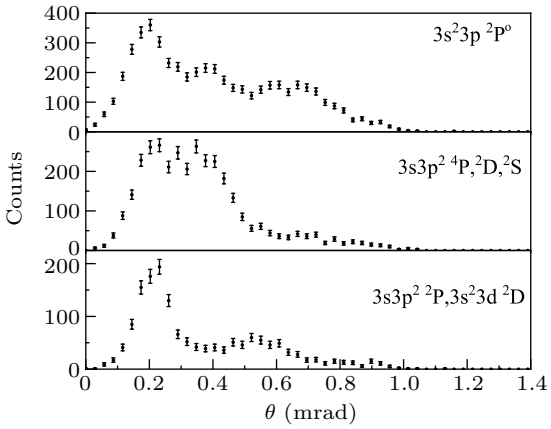


Fig. 6. Measured angular distributions in the final states of the DEC process at 100 keV collision energy.

4. Conclusions

The SEC and DEC processes for the low-energy S^{5+}–He collision were studied at impact energies from 50.8 keV to 100 keV. In the SEC process, the direct capture of single electrons into 3s, 3p, 3d orbitals and transfer projectile excitation of the $3p^2$ process dominate. Realizations with ^{2S+1}L resolution such as 3s3p ^{3}P^o, 3s3p ^{1}P^o, etc. were achieved. As the collision energy increases, the channels for captured electrons to higher excited states are opened and the proportion of captured electrons going to the $3s^2$ ground state increases slightly. For the DEC process, the captured electrons preferentially populate the ground state $3s^2 3p\ ^2$P, while the aggregation of captured electrons to the $3s3p^2$ state is of secondary importance. As the collision energy increases, the entry of captured electrons into higher excited states becomes increasingly important. The reaction windows calculated using the MCBM model can qualitatively interpret the measured state-population distributions for SEC and DEC. The scattering angular distributions show the bimodal and multi-modal structures of SEC and DEC, respectively. Future theoretical studies are required to provide a more comprehensive interpretation of the experimental findings.

Data availability statement

The data that support the findings of this study are openly available in Science Data Bank at the following link https://doi.org/10.57760/sciencedb.j00113.00233.

Acknowledgments

Project supported by the National Key Research and Development Program of China (Grant No. 2022YFA1602500) and the National Natural Science Foundation of China (Grant No. 11974358). The authors would like to thank the staff of 320 kV and EBIS platforms for their technical support.

References

[1] Ullrich J, Moshammer R, Dorner R, Jagutzki O, Mergel V, Schmidt-Bocking H and Spielberger L 1997 *J. Phys. B: At. Mol. Opt. Phys.* **30** 2917
[2] Cravens T E 2002 *Science* **296** 1042
[3] Isler R C 1994 *Plasma Phys. Control. Fusion* **36** 171
[4] Gervais B, Beuve M, Olivera G and Galassi M 2006 *Radiat. Phys. Chem.* **75** 493
[5] Wei B R and Zhang R T 2025 *Sci. Sin. Phys. Mech. Astron.* **55** 250008
[6] Ma X, Zhang S, Wen W, Huang Z, Hu Z, Guo D, Gao J, Najjari B, Xu S, Yan S, Yao K, Zhang R, Gao Y and Zhu X 2022 *Chin. Phys. B* **31** 093401
[7] Zhang R T, Gao J W, Zhang Y W, Guo D L, Gao Y, Zhu X L, Xu J W, Zhao D M, Yan S, Xu S, Zhang S F, Wu Y, Wang J G and Ma X 2023 *Phys. Rev. Res.* **5** 023123
[8] Ma P F, Wang J R, Zhang Z X, Meng T M, Xia Z H, Ren B H, Wei L, Yao K, Xiao J, Zou Y M, Tu B S and Wei B R 2023 *Nucl. Sci. Tech.* **34** 156
[9] Cao T, Meng T, Gao Y, Zhang S F, Zhang R T, Yan S, Zhu X L, Wang J, Ma P, Ren B, Xia Z H, Guo D L, Zhang C J, Lin K Z, Xu S, Wei B and Ma X 2023 *Astrophys. J. Suppl. Ser.* **266** 20
[10] Zhu X B, Xing D D, Lin K Z, Cui S C, Zhu X L, Gao Y, Guo D L, Zhao D M, Zhang S F and Ma X 2024 *J. Phys. B: At. Mol. Opt. Phys.* **57** 045001
[11] Wu Y J, Meng T M, Zhang X W, Tan X, Ma P F, Yin H, Ren B H, Tu B S, Zhang R T, Xiao J, Ma X W, Zou Y M and Wei B R 2024 *Acta Phys. Sin.* **73** 240701 (in Chinese)
[12] Lin K Z, Gao Y, Zhu X L, Zhang S F, Cao T, Guo D L, Shan X, Zhao D M, Chen X J and Ma X 2024 *Phys. Rev. A* **109** 052811
[13] Siddiki M A K A, Zhao G P, Liu L and Misra D 2024 *Phys. Rev. A* **109** 032819
[14] Ma M X, Meng T, Tu B, Ma P, Zhang Y W, Liu L, Xiao J, Yao K, Zou Y, Wu Y, Wang J G and Wei B 2024 *Phys. Rev. A* **110** 032806
[15] Zhu X, Zhang S, Gao Y, Guo D, Xu J, Zhang R, Zhao D, Lin K, Zhu X, Xing D, Cui S, Passalidis S, Dubois A and Ma X 2024 *Phys. Rev. Lett.* **133** 173002
[16] Zhu X B, Zhang R T, Zhang C J, Mitrani S, Gu L, Gao Y, Zhang S F and Ma X 2025 *Astrophys. J. Suppl. Ser.* **277** 35
[17] Liu L, Wu Y, Wang J and Janev R 2022 *At. Data Nucl. Data Tables* **143** 101464
[18] Gao J W, Wu Y, Sisourat N, Wang J G and Dubois A 2017 *Phys. Rev. A* **96** 052703
[19] Zhang Y W, Gao J W, Wu Y, Wang J G, Sisourat N and Dubois A 2022 *Phys. Rev. A* **106** 042809
[20] Lanzerotti L J, Armstrong T P, Gold R E, Anderson K A, Krimigis S M, Lin R P, Pick M, Roelof E C, Sarris E T, Simnett G M, Maclennan C G, Choo H T and Tappin S J 1992 *Science* **257** 1518

[21] Frankel M, Beiersdorfer P, Brown G V, Gu M F, Kelley R L, Kilbourne C A and Porter F S 2009 *Astrophys. J.* **702** 171

[22] Clark G, Mauk B H, Paranicas C, Kollmann P and Smith H T 2016 *J. Geophys. Res. Space Phys.* **121** 2264

[23] Mifsud D V, Kaňuchová Z, Herczku P, Ioppolo S, Juhász Z, Kovács S T S, Mason N J, McCullough R W and Sulik B 2021 *Space Sci. Rev.* **217** 14

[24] Boyarsky A, Ruchayskiy O, Iakubovskyi D and Franse J 2014 *Phys. Rev. Lett.* **113** 251301

[25] Bulbul E, Markevitch M, Foster A, Smith R K, Loewenstein M and Randall S W 2014 *Astrophys. J.* **789** 13

[26] Wilson S M, McLaughlin T K, McCullough R W and Gilbody H B 1990 *J. Phys. B: At. Mol. Opt. Phys.* **23** 2969

[27] Zhao L B, Stancil P C, Gu J P, Hirsch G, Buenker R J, Imai T W and Kimura M 2005 *Phys. Rev. A* **72** 032719

[28] Wilson S M, McLaughlin T K, McCullough R W and Gilbody H B 1990 *J. Phys. B: At. Mol. Opt. Phys.* **23** 1315

[29] Bacchus-Montabonel M 1998 *Chem. Phys.* **228** 181

[30] Labuda M, Tergiman Y, Bacchus-Montabonel M and Sienkiewicz J 2004 *Int. J. Mol. Sci.* **5** 265

[31] Labuda M, Tergiman Y, Bacchus-Montabonel M C and Sienkiewicz J 2004 *Chem. Phys. Lett.* **394** 446

[32] Wang J G, Turner A R, Cooper D L, Schultz D R, Rakovic M J, Fritsch W, Stancil P C and Zygelman B 2002 *J. Phys. B: At. Mol. Opt. Phys.* **35** 3137

[33] Dörner R, Mergel V, Jagutzki O, Spielberger L, Ullrich J, Moshammer R and Schmidt-Böcking H 2000 *Phys. Rep.* **330** 95

[34] Zhu X, Cui S, Xing D, Xu J, Najjari B, Zhao D, Guo D, Gao Y, Zhang R, Su M, Zhang S and Ma X 2024 *Chin. Phys. B* **33** 023401

[35] Niehaus A 1986 *J. Phys. B: At. Mol. Phys.* **19** 2925

[36] Zhu X, Ma X, Li J, Schmidt M, Feng W, Peng H, Xu J, Zschornack G, Liu H, Zhang T, Zhao D, Guo D, Huang Z, Zhou X, Gao Y, Cheng R, Wang H, Yang J and Kang L 2019 *Nucl. Instrum. Methods Phys. Res. B* **460** 224

[37] Ma X, Zhang R T, Zhang S F, Zhu X L, Feng W T, Guo D L, Li B, Liu H P, Li C Y, Wang J G, Yan S C, Zhang P J and Wang Q 2011 *Phys. Rev. A* **83** 052707

[38] Xu J W, Xu C X, Zhang R T, Zhu X L, Feng W T, Gu L, Liang G Y, Guo D L, Gao Y, Zhao D M, Zhang S F, Su M G and Ma X 2021 *Astrophys. J. Suppl. Ser.* **253** 13

[39] Yuan H, Xu S, Wang E, Xu J, Gao Y, Zhu X, Guo D, Ma B, Zhao D, Zhang S, Yan S, Zhang R, Gao Y, Xu Z and Ma X 2022 *J. Phys. Chem. Lett.* **13** 7594

[40] Cui S, Xing D, Zhu X, Su M, Gao Y, Guo D, Zhao D, Zhang S, Fu Y and Ma X 2024 *Chin. Phys. B* **33** 073401

[41] Fischer D, Feuerstein B, DuBois R D, Moshammer R, López-Urrutia J R C, Draganić I, Lörch H, Perumal A N and Ullrich J 2002 *J. Phys. B: At. Mol. Opt. Phys.* **35** 1369

[42] Buenker R J and Phillips R A 1985 *J. Mol. Struct. THEOCHEM* **123** 291

[43] Krebs S and Buenker R J 1995 *J. Chem. Phys.* **103** 5613

[44] Zygelman B, Cooper D L, Ford M J, Dalgarno A, Gerratt J and Raimondi M 1992 *Phys. Rev. A* **46** 3846

[45] Bransden B H and McDowell M R C 1992 *Charge Exchange and the Theory of Ion-Atom Collisions* (Oxford: Oxford University Press)

[46] Nolte J L, Stancil P C, Liebermann H P, Buenker R J, Hui Y and Schultz D R 2012 *J. Phys. B: At. Mol. Opt. Phys.* **45** 245202

[47] Wang X X, Wang K, Peng Y G, Liu C H, Liu L, Wu Y, Liebermann H P, Buenker R J and Qu Y Z 2021 *Chin. Phys. Lett.* **38** 113401